Magnetotransport at Domain Walls in $BiFeO_3$

Q. He,[1,2] C.-H. Yeh,[3] J.-C. Yang,[4] G. Singh-Bhalla,[1] C.-W. Liang,[1] P.-W. Chiu,[3] G. Catalan,[5] L. W. Martin,[6] Y.-H. Chu,[1,4,7,*] J. F. Scott,[8] and R. Ramesh[1,7]

[1]*Department of Physics, University of California, Berkeley, California 94720, USA*
[2]*Advanced Light Source, Lawrence Berkeley National Laboratory, Berkeley, California 94720, USA*
[3]*Department of Electrical Engineering, National Tsing Hua University, Hsinchu 30013, Taiwan*
[4]*Department of Materials Science and Engineering, National Chiao Tung University, HsinChu 30010, Taiwan*
[5]*Institució Catalana de Recerca i Estudis Avanats (ICREA) and Centre d'Investigació en Nanociència i Nanotecnologia (CIN2), Campus Universitat Autònoma de Barcelona, Bellaterra, Spain*
[6]*Department of Materials Science and Engineering and Materials Research Laboratory, University of Illinois, Urbana-Champaign, Urbana, Illinois 61801, USA*
[7]*Department of Materials Science and Engineering, University of California, Berkeley, California 94720, USA*
[8]*Cavendish Laboratory, Department of Physics, Cambridge University, Cambridge CB3 0HE, United Kingdom*

(Received 4 August 2011; published 9 February 2012)

Domain walls in multiferroics can exhibit intriguing behaviors that are significantly different from the bulk of the material. We investigate strong magnetoresistance in domain walls of the model multiferroic $BiFeO_3$ by probing ordered arrays of 109° domain walls with temperature- and magnetic-field-dependent transport. We observe temperature-dependent variations in the transport mechanism and magnetoresistances as large as 60%. These results suggest that by locally breaking the symmetry of a material, such as at domain walls and structural interfaces, one can induce emergent behavior with properties that deviate significantly from the bulk.

DOI: 10.1103/PhysRevLett.108.067203 PACS numbers: 75.60.Ch, 75.47.Lx, 75.85.+t

Interfaces have emerged as a key focal point of condensed matter science. In correlated oxides, heterointerfaces provide a powerful route to create and manipulate charge, spin, orbital, and lattice degrees of freedom [1]. In ferroelectrics, domain walls emerge as natural interfaces resulting from the minimization of electrostatic and/or elastic energies. Pioneering symmetry analyses by Janovec and co-workers suggest that domain walls in multiferroics can manifest a net magnetic moment even if the domains themselves are antiferromagnetic or paramagnetic [2,3]. Likewise, spin rotations across domain walls in magnetic insulators can induce a polarization in the walls of otherwise nonpolar materials [4,5] and coupled behavior at domain walls has been shown in classic antiferromagnets such as $GdFeO_3$ [6]. The work of Lajzerowicz and Niez [7] identified the possibility of phase transitions at domain walls in ferroic systems, an aspect that was further illustrated in the seminal work of Aird *et al*. [8] who showed the possibility of superconductivity at twin boundaries in WO_3. A recent study on $YMnO_3$ by Choi *et al*. has addressed the formation of insulating paraelectric states at domain walls [9].

Among the large number of materials systems currently being explored, the model ferroelectric-antiferromagnet $BiFeO_3$ (BFO) has captured a significant amount of research attention, since the two primary order parameters are robust with respect to room temperature ($T_C \sim 830\,^\circ$C, $T_N \sim 380\,^\circ$C) [10,11]. Some studies [12,13] have suggested the importance of certain types of domain walls (i.e., 109° walls) in determining the nature of exchange bias coupling between BFO and ferromagnetic layers. The recent atomic force microscopy (AFM)-based observation of enhanced electrical conduction at certain types of ferroelectric domain walls in BFO [14,15] provides another important example of the connection between atomic, electronic, and magnetic structure in domain walls of these complex materials. However, such scanning probe microscopy-based measurements can take us only so far in understanding the fundamental physics at these domain walls.

With this as the background, we explore here the temperature- and magnetic-field-dependent transport at ferroelectric domain walls in BFO thin films with controlled 109° domain wall structures [16]. For this study, epitaxial 100 nm $BFO/DyScO_3$ $(110)_O$ heterostructures were grown using pulsed laser deposition. Both out-of-plane (OOP) and lateral, in-plane (IP) piezoresponse force microscopy (PFM) images of the 109° domain wall samples show stripelike contrast [Figs. 1(a) and 1(b), respectively]. The OOP PFM image shows two contrast levels, dark and bright [Fig. 1(a)], corresponding to the OOP component of the polarization alternating between down and up directions, while the IP-PFM image [Fig. 1(b)] has three contrast levels dark (black), neutral (brown), and bright (white). Dark and bright contrast correspond to the IP component of the polarization pointing along $[1\bar{1}0]_{pc}$ and $[\bar{1}10]_{pc}$ in different ferroelectric domains as shown in Fig. 1(c), while neutral contrast corresponds to the IP component of the polarization pointing either along $[\bar{1}\bar{1}0]_{pc}$ or $[110]_{pc}$. Atomic

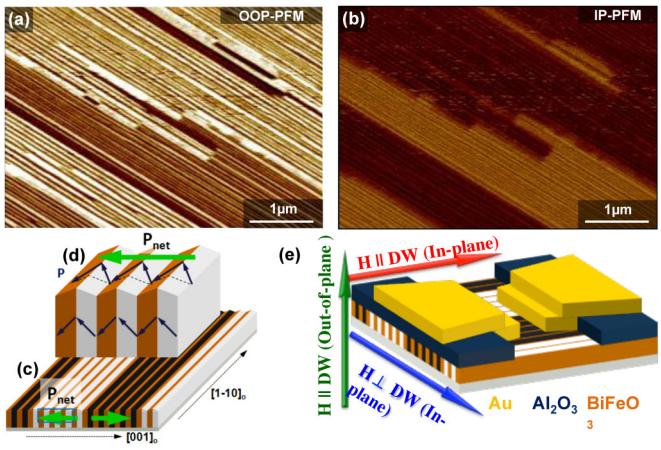

FIG. 1 (color online). Domain structures in $BiFeO_3$ on 109° domain wall samples. (a),(b) OOP- and IP-PFM images of 109° domain pattern. (c) Schematic of 109° domain pattern with different domain clusters. Domain colors follow the contrast of the IP-PFM image as shown in (b). The green arrow shows the net ferroelectric polarization within each domain cluster. (d) Schematic of detailed 109° domain structure within one domain cluster. Blue (or dark gray) arrows show the ferroelectric polarization components in $[001]_{pc}$ and $[010]_{pc}$ planes. (e) Schematic of the device structure, an example of current path parallel to the domain walls.

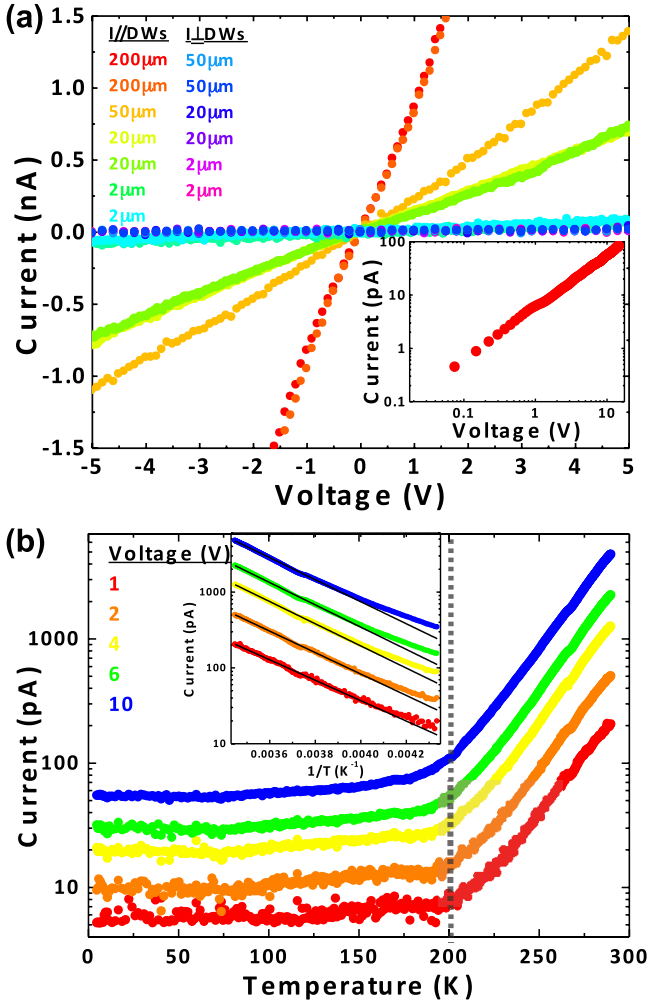

FIG. 2 (color online). Transport study on 109° domain wall samples. (a) Room temperature *I-V* curves with different device geometry. The inset shows the corresponding *I-V* curve (plotted in log-log scale) measured at 3 K of the same device used in (b). (b) Current-temperature curves with various voltage bias. The inset of this figure is a blowup plot of the data within the high temperature regime (> 200 K). The temperature axis has been plotted as 1/T in order to show the exponential fits (black lines) of the curves.

resolution transmission electron microscopy images, obtained using the aberration-corrected microscope (TEAM 0.5) at the National Center for Electron Microscopy, reveal the atomically sharp structure of such walls. These images (e.g., Supplemental Material, Fig. S1 [17]) show that the 109° domain walls are ~1–2 nm (3–5 unit cells) wide and, indeed, form on the 100-type planes as expected from the literature [18].

In order to investigate the temperature- and magnetic-field-dependent transport properties of these domain walls, test structures for in-plane transport measurements were fabricated using photolithography techniques [devices are schematically illustrated in Fig. 1(e)]. These structures were fabricated by first depositing a 10 nm insulating Al_2O_3 buffer layer with open windows for the electrodes and current path and subsequent deposition of 20 nm Ti/150 nm Au electrodes with a critical feature separation of 0.75–1.5 μm. Such an electrode structure allowed for a controlled contact area to the domain wall arrays. These electrode patterns were defined by e-beam lithography with a lift-off process. An oxygen plasma process was applied to clean the photoresist residue in the contact area before the Ti/Au deposition. The electrodes were fabricated in two geometries relative to the domain wall directions, i.e., current paths parallel [Fig. 1(e)] or perpendicular to the domain walls. The test system and the equivalent circuit are described in the Supplemental Material, Figs. S2(a) and S2(b) [17]. We observe a strong anisotropy of transport between transport parallel and perpendicular to the walls [Fig. 2(a)]. Current-voltage (*I-V*) curves for test structures with 2–200 μm contact lengths are shown in Fig. 2(a) and illustrate the scaling of the total current with the number of domain walls included in the transport path. With the electrode pair perpendicular to the domain walls, we consistently observe resistance values that are 50–200 times higher than the transport parallel to the walls. Based on a simple parallel and series resistor model (described in detail in the Supplemental Material, document S3 [17]), we estimate the resistivity of the wall (~ 100 $\Omega \cdot$ m) to be 4 orders of magnitude lower than the domain, consistent with our previous measurements on single domain walls [14,19,20]. Therefore, we conclude that the 109° domain

walls are the main current paths connecting the in-plane electrodes.

We then proceeded to measure the temperature (3–300 K) dependence of transport with the current transport parallel to the 109° domain walls. The voltage-dependent, current-temperature plots in Fig. 2(b) reveal two distinct regimes. Above 200 K, the transport can be described by a thermally activated behavior as shown in the inset of Fig. 2(b) for several constant voltage sweeps, with an activation energy of ~0.25 eV. Supplemental Material, Fig. S4 [17] shows similar data from five different samples to illustrate the repeatability of the measurement. This transition in transport behavior at ~200 K is intriguing, particularly since phase transitions in $BiFeO_3$ near 200 K have been observed in other work [21]. The activation energy of 0.25 eV estimated from fitting the experimental data [Fig. 2(b), inset] is also in close agreement with AFM-based measurements of thermally activated transport through such walls [22]. It is also consistent with recent calculations of oxygen vacancy trap states in BFO [23], suggesting that it could be arising from detrapping of carriers from oxygen vacancies. Below ~200 K, the transport is, surprisingly, only weakly temperature dependent. We have explored various possible transport mechanisms to describe this behavior. Using the knowledge of transport in other Fe-based oxides as a background [24–26], it is tempting to ascribe this behavior to a variable range hopping (VRH) process [24]. However, the absence of a significant change in the resistance with lowering temperature seems to preclude such a process. Another possible transport process can be direct tunneling, which typically manifests as a weak temperature dependence. However, the inset to Fig. 2(a) shows linear *I*-*V* behavior at 3 K, negating this possibility. Given that negative magnetoresistance (MR) (shown in the following paragraphs) is observed below 200 K only, we speculate that transport at low temperatures is influenced by spin dependent scattering mechanisms. Additional studies are required to further explore the transport mechanisms at low temperature.

We next turn to the magnetic field dependence of the transport behavior. First, all the samples studied exhibited a marked, negative MR when both magnetic field and transport were parallel to the walls [black curves, Fig. 3(a)]. Negative MR values as high as ~60% were obtained at a magnetic field of 7 T. Strikingly, when the magnetic field was applied perpendicular to the transport path [both in-plane (green) and out-of-plane (blue)] or when the transport is perpendicular to the walls, little MR is observed, indicating that the MR is directly related to the preferential transport parallel to the walls. The temperature-dependent resistance and *I*-*V* behavior of similar devices were also measured under two different magnetic fields, 0 T and 8 T [blue and red curves in Fig. 3(b), respectively]. The inset shows linear *I*-*V* plots with and without the magnetic field. Negative MR is only observed for temperatures below the

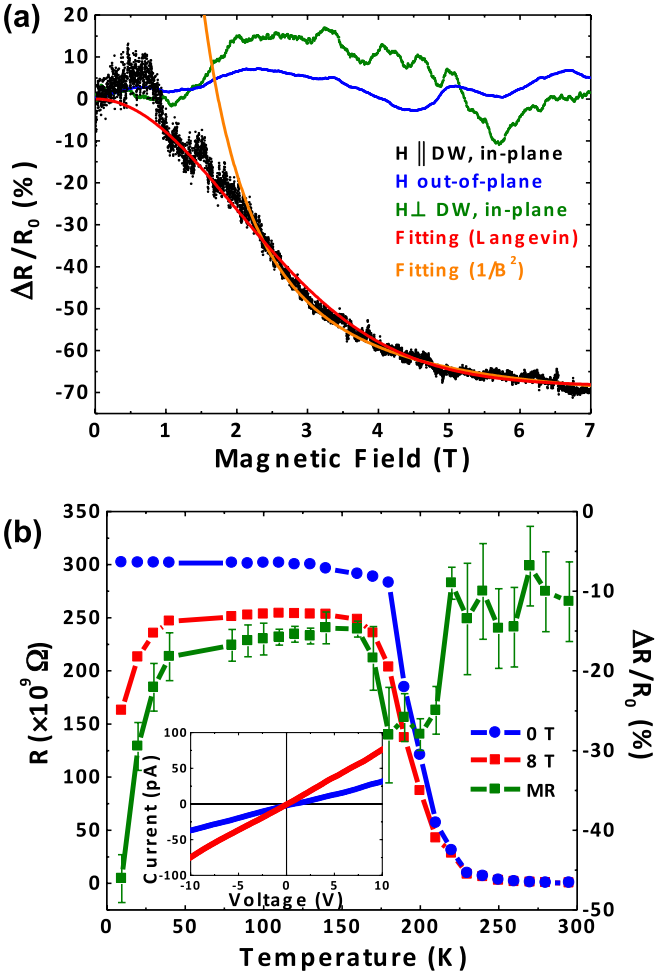

FIG. 3 (color online). Magnetotransport study on 109° domain wall samples. (a) Anisotropic magnetoresistance in different directions of external magnetic field as illustrated in Fig. 1(e) at a temperature of 10 K. (b) Resistance-temperature curves at two different external magnetic fields showing in red (8 T) and blue (0 T). The corresponding magnetoresistance is shown in green.

transition temperature (~ 200 K), which suggests that magnetic interactions are likely to play a key role in influencing the observed transport behavior. Moreover, below 40 K, the magnitude of MR gets significantly larger, from ~20% at ~100 K to ~60% at ~10 K.

In strongly correlated systems, such as manganites, several mechanisms have been invoked to explain the transport behavior and the negative magnetoresistance [27–29]. A general theme in all of the models is the magnetic field dependence of the core spin orientation and its influence on electron transport. Given the complex nature of magnetism at the 109° domain wall in BFO, we have chosen to explore empirical analyses of the MR vs B data in Fig. 3(a) using (1) a model that approximates the domain walls as sheets that exhibit an enhanced magnetic moment, and (2) a model that assumes the presence of spin clusters within the domain walls and electron

tunneling or hopping across the clusters [30,31]. In the first model, the magnetic field dependence of the magnetic moment in the wall is approximated by a classical Langevin function

$$M = L\left(\frac{\mu B}{k_B T}\right)$$

where $L(x) = \coth(x) - 1/x$ [32,33]. This simple picture of the magnetic state in the domain wall is then used within a model of spin dependent scattering of the transport process [24]

$$I = I_0 \exp\left\{-\frac{\Delta W}{k_B T}\right\}$$

to help explain the field dependence of the MR. A detailed analysis is presented in the Supplemental Material, document 5 [17]. The model calculation, shown in Fig. 3(a), shows a decent fit to the experimental data, suggesting this as a possible mechanism to explain our MR vs H behavior.

For the second case considered above, we expect a dependence of the form

$$\frac{\rho(B) - \rho(0)}{\rho(0)} = AB^{-2} + C.$$

While this model appears to fit the experimental data quite well at higher fields (i.e., above a few Tesla), the fit is not as good at lower fields.

While both models reasonably describe the data, we note that a precise picture of the magnetic state in the wall is likely to be a bit more complicated. It is, however, important to note that this magnetic state is significantly different from that of the bulk of BFO (namely, a weakly canted antiferromagnet). Indeed, this difference in the magnetic state within the domain wall is reflected in several other measurements, including a measurable x-ray magnetic circular dichroism in samples with a high density of such 109° domain walls, and a strong exchange bias coupling to a ferromagnetic overlayer [34]. In summary, we have systematically studied the temperature- and magnetic-field-dependent transport in BFO thin films possessing arrays of 109° ferroelectric domain walls. A clear demonstration of the anisotropy in transport parallel and perpendicular to the walls has been observed. By far, the most interesting aspect of the research presented in this Letter is the large MR behavior at such walls; the trends are reminiscent of the colossal magnetoresistance effects observed in the bulk in doped manganites. Does the electronic and magnetic properties of the almost 2D domain wall mimic that of the electronically phase separated manganite system? Clearly, the limits of this behavior need to be determined with further work.

The work at Berkeley is partially supported by the Director, Office of Science, Office of Basic Energy Sciences, Materials Sciences Division of the U.S. Department of Energy under Contract No. DE-AC02-05CH11231. Y. H. C. also acknowledges the support of the National Science Council, R.O.C., under Contract No. NSC 100-2119-M-009-003. L. W. M acknowledges support from the Army Research Office under Grant No. W911NF-10-1-0482. Partial support of NDSEG and from the NSF-MRSEC are gratefully acknowledged.

*yhc@cc.nctu.edu.tw

[1] S. M. Wu, S. A. Cybart, P. Yu, M. D. Rossell, J. X. Zhang, R. Ramesh, and R. C. Dynes, Nature Mater. **9**, 756 (2010).
[2] J. Přívratská and V. Janovec, Ferroelectrics **204**, 321 (1997).
[3] J. Přívratská and V. Janovec, Ferroelectrics **222**, 23 (1999).
[4] M. Fiebig, Adv. Solid State Phys. **46**, 255 (2007).
[5] M. Mostovoy, Phys. Rev. Lett. **96**, 067601 (2006).
[6] Y. Tokunaga, N. Furukawa, H. Sakai, Y. Taguchi, T. hisa Arima, and Y. Tokura, Nature Mater. **8**, 558 (2009).
[7] J. Lajzerowicz and J. J. Niez, J. Phys. Lett. **40**, 165 (1979).
[8] A. Aird and E. K. H. Salje, J. Phys. Condens. Matter **10**, L377 (1998).
[9] T. Choi, Y. Horibe, H. T. Yi, Y. J. Choi, W. Wu, and S.-W. Cheong, Nature Mater. **9**, 253 (2010).
[10] Y. E. Roginska, Y. Y. Tomashpolsky, Y. N. Venevtsev, V. M. Petrov, and G. S. Zhdanov, Sov. Phys. JETP **23**, 47 (1966).
[11] S. V. Kiselev, R. P. Ozerov, and G. S. Zhdanov, Sov. Phys. Dokl. **7**, 742 (1963).
[12] H. Béa, M. Bibes, F. Ott, B. Dupé, X.-H. Zhu, S. Petit, S. Fusil, C. Deranlot, K. Bouzehouane, and A. Barthélémy, Phys. Rev. Lett. **100**, 017204 (2008).
[13] L. W. Martin, Y.-H. Chu, M. B. Holcomb, M. Huijben, P. Yu, S.-J. Han, D. Lee, S. X. Wang, and R. Ramesh, Nano Lett. **8**, 2050 (2008).
[14] J. Seidel *et al.*, Nature Mater. **8**, 229 (2009).
[15] S. Farokhipoor and B. Noheda, Phys. Rev. Lett. **107**, 127601 (2011).
[16] Y.-H. Chu, Q. He, C.-H. Yang, P. Yu, L. W. Martin, P. Shafer, and R. Ramesh, Nano Lett. **9**, 1726 (2009).
[17] See Supplemental Material at http://link.aps.org/supplemental/10.1103/PhysRevLett.108.067203 for more detailed experimental and analysis information about this work.
[18] S. K. Streiffer, C. B. Parker, A. E. Romanov, M. J. Lefevre, L. Zhao, J. S. Speck, W. Pompe, C. M. Foster, and G. R. Bai, J. Appl. Phys. **83**, 2742 (1998).
[19] G. W. Pabst, L. W. Martin, Y. H. Chu, and R. Ramesh, Appl. Phys. Lett. **90**, 072902 (2007).
[20] S. R. Basu, L. W. Martin, Y.-H. Chu, M. Gajek, R. Ramesh, R. C. Rai, X. Xu, and J. L. Musfeldt, Appl. Phys. Lett. **92**, 091905 (2008).
[21] M. K. Singh, R. S. Katiyar, and J. F. Scott, J. Phys. Condens. Matter **20**, 252203 (2008).
[22] J. Seidel *et al.*, Phys. Rev. Lett. **105**, 197603 (2010).
[23] S. J. Clark and J. Robertson, Appl. Phys. Lett. **94**, 022902 (2009).
[24] N. F. Mott and E. A. Davis, *Electronic Processes in Non-crystalline Materials* (Clarendon Press, Oxford, 1979).

[25] M. Hasegawa, J. Yanagihara, Y. Toyoda, E. Kita, and L. Ranno, J. Magn. Magn. Mater. **310**, 2283 (2007).
[26] J. C. Papaioannou, G. S. Patermarakis, and H. S. Karayianni, J. Phys. Chem. Solids **66**, 839 (2005).
[27] E. Dagotto, *Nanoscale Phase Separation and Colossal Magnetoresistance* (Springer, New York, 2003).
[28] E. L. Nagaev, Phys. Rep. **346**, 387 (2001).
[29] M. B. Salamon and M. Jaime, Rev. Mod. Phys. **73**, 583 (2001).
[30] N. A. Babushkina, E. A. Chistotina, K. I. Kugel, A. L. Rakhmanov, O. Y. Gorbenko, and A. R. Kaul, J. Phys. Condens. Matter **15**, 259 (2003).
[31] K. I. Kugel, A. L. Rakhmanov, A. O. Sboychakov, M. Yu. Kagan, I. V. Brodsky, and A. V. Klaptsov, in *Physics of Spin in Solids: Materials, Methods and Applications*, edited by S. Halilov, NATO Science Series (Kluwer, Dordrecht, 2004), Vol. 156, pp. 177–194.
[32] R. C. O'Handley, *Modern Magnetic Materials* (Wiley-Interscience, New York, 1999).
[33] E. Dagotto, T. Hotta, and A. Moreo, Phys. Rep. **344**, 1 (2001).
[34] Q. He, A. Scholl, E. Arenholz, Y.-H. Chu, and R. Ramesh, [Phys. Rev. Lett. (to be published)].